Dissipation of angular momentum in light heavy-ion collision

C. Bhattacharya, S. Bhattacharya, T. Bhattacharjee, A. Dey, S. Kundu, S. R. Banerjee, P. Das, S. K. Basu, and K. Krishan
Variable Energy Cyclotron Centre, 1/AF Bidhan Nagar, Kolkata 700 064, India

The inclusive energy distributions of fragments ($4 \leq Z \leq 7$) emitted in the reactions ^{16}O(116 MeV)$+^{27}$Al, ^{28}Si, ^{20}Ne(145 MeV)$+^{27}$Al, ^{59}Co have been measured in the angular range $\theta_{lab}=10°-65°$. The respective fusion-fission and deep inelastic contributions have been decomposed from the experimental fragment energy spectra. The angular momentum dissipations in fully damped deep inelastic collisions have been estimated assuming exit channel configuration similar to those for fusion-fission process. It has been found that, the angular momentum dissipations are more than those predicted by the empirical sticking limit in all cases. The deviation is found to increase with increasing charge transfer (lighter fragments). Qualitatively, this may be due to stronger friction in the exit channel. Moreover, for the heavier system ^{20}Ne$+^{59}$Co, the overall magnitude of deviation is less as compared to those for the lighter systems, i.e., ^{16}O$+^{27}$Al, ^{28}Si, ^{20}Ne$+^{27}$Al. This may be due to lesser overlap in time scales of fusion and deep inelastic time scales for heavier systems.

I. INTRODUCTION

Several experimental studies have been made in the recent years to understand the reaction mechanism of fragment emission in light heavy ion collisions [1–15] at low bombarding energies ($\lesssim$10 MeV/nucleon). The fragments (mostly binary in nature at these energies) are emitted with different degree of dissipation of the entrance channel kinetic energy between the two colliding ions —ranging from quasielastic to deep inelastic (DI) to the fully relaxed fusion-fission (FF) processes. Thus the fragments carry the signatures of nuclear dissipation, which, if deciphered, may bring out valuable information on the nature of nuclear dissipation.

In addition to kinetic energy dissipation, dissipative heavy-ion collision processes also result in significant dissipation of relative angular momentum in the entrance channel. Phenomenologically, the kinetic energy dissipation originates from friction (radial and tangential) between the surfaces of the rotating dinuclear system; on the other hand, angular momentum dissipation is decided solely by the tangential component of the friction, and the magnitude of dissipation is expected to lie between two limits (rolling and sticking). However, very large dissipation of relative angular momentum in excess of the sticking limit predictions has also been reported in the literature [12]. This anomaly, as pointed out by several authors [10,14,16–18], is due to the ambiguity in the determination of the magnitude of angular momentum dissipation (and vis-a-vis the rotational contribution to the fragment kinetic energy). Estimation of the angular momentum in the exit channel is strongly dependent on another poorly known factor, i.e., the scission configuration of the rotating dinuclear system. This apparently hinted at the incompleteness of our understanding of the dynamics of nuclear dissipation process, which prompted us to make a systematic study of angular momentum dissipation in light nuclear systems where Coulomb and rotational contributions to the fragment kinetic energies are comparable.

It is clear from the above that an independent estimation of the scission configuration is necessary to make a proper estimate of the angular momentum transfer. Generally, it is estimated from the total kinetic energy of the rotating dinuclear system, E_k, which is given by

$$E_k = V_N(d) + f^2 \frac{\hbar^2 l_i(l_i+1)}{2\mu d^2}, \qquad (1)$$

where $V_N(d)$ is the contribution from Coulomb and nuclear forces at dinuclear separation distance d, μ is the reduced mass of the dinuclear configuration, l_i is the relative angular momentum in the entrance channel, and f is the numerical factor denoting the fraction of the angular momentum transferred depending on the type of frictional force. Since it is not possible to determine both f and d by solving Eq. (1), in the earlier works, one of them was estimated phenomenologically (usually for f, its value corresponding to sticking limit was taken) and the other was estimated from the experimental fragment kinetic energy data using Eq. (1). It is however well known (see, for example, Ref. [1] and references therein) that, apart from dissipative collision process, fusion-fission process also contributes significantly in the fragment emission scenario. Thus, it is required to estimate and separate out the FF part of the fragment energy spectra in order to extract the kinetic energy distribution of the DI part of the rotating dinuclear system. In the present work, we have studied fragment emission from ^{16}O(116 MeV)$+^{27}$Al, ^{28}Si, ^{20}Ne(145 MeV)$+^{27}$Al, ^{59}Co and report on how angular momentum dissipation can be estimated from the FF and DI components extracted by nonlinear optimization procedure using multiple Gaussians [1]. Some parts of the ^{16}O(116 MeV)$+^{27}$Al data have already been published in Ref. [1], where it has been shown that the FF component is quite competitive, in agreement with the previous work [19].

The paper has been organized as follows. Experimental details and results have been described in Sec. II. Discussions of the results have been given in Sec. III. Finally, the summary and concluding remarks have been given in Sec. IV.
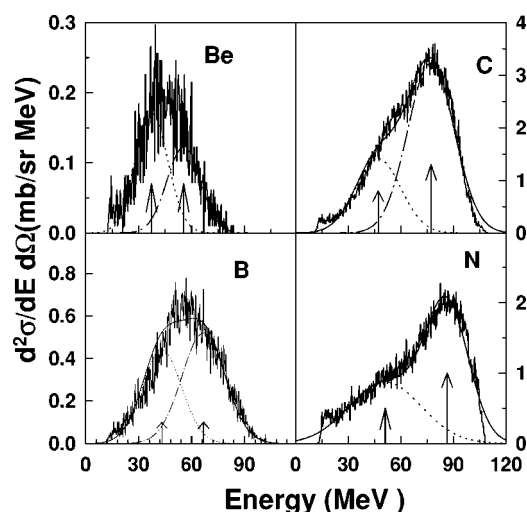
FIG. 1. Typical energy spectra of different fragments obtained at 15° for the $^{16}O+^{27}Al$ reaction. Dotted, dash-dotted, and solid curves represent contributions of FF, DI, and their sum (FF+DI), respectively. Left and right arrows correspond to the centroids of FF and DI energy distributions, respectively.

II. EXPERIMENTS AND RESULTS

The experiment was performed using 116 MeV $^{16}O^{5+}$ and 145 MeV $^{20}Ne^{6+}$ ion beams from the variable energy cyclotron at Kolkata. Self-supporting targets of 420 $\mu g/cm^2$ ^{27}Al, ~1 mg/cm^2 ^{28}Si, and ~2 mg/cm^2 ^{59}Co were used in the experiment. The fragments were detected using three solid state [Si(SB)] telescopes (~12 μm ΔE, 300 μm E) mounted on one arm of the 91.5 cm scattering chamber. Typical solid angle subtended by each detector was ~0.3 msr. A monitor detector [~300 μm Si(SB)] was placed on the other arm of the scattering chamber for normalization purpose. The telescopes were calibrated using elastically scattered ^{16}O and ^{20}Ne ions from Au target and α particles from (^{229}Th-α) source. Energy losses of the incoming beam as well as the outgoing fragments in the target have been properly taken care of.

Inclusive energy distributions for various fragments ($4 \leqslant Z \leqslant 7$) were measured in the angular range $10°-65°$. Typical energy spectra of the fragments ($4 \leqslant Z \leqslant 7$) emitted in the reaction $^{16}O(116 \text{ MeV})+^{27}Al$ have been shown in Fig. 1 for $\theta_{lab}=15°$. The systematic errors in the data, arising from the uncertainties in the measurements of solid angle, target thickness and the calibration of current digitizer have been estimated to be $\approx 10\%$.

a. Decomposition of FF and DI components. The contributions of fusion-fission and DI components are estimated by fitting the measured spectra with Gaussian functions as per the procedure laid down in Ref. [1]. The energy spectra of different fragments at each angle have been fitted with two Gaussian functions in two steps. In the first step, the FF contributions have been obtained by fitting the energy distributions with a Gaussian having centroid at the energies obtained from Viola systematics [20], adapted for light nuclear systems [21], of total kinetic energies of mass-symmetric fission fragments duly corrected for asymmetric factor [5].
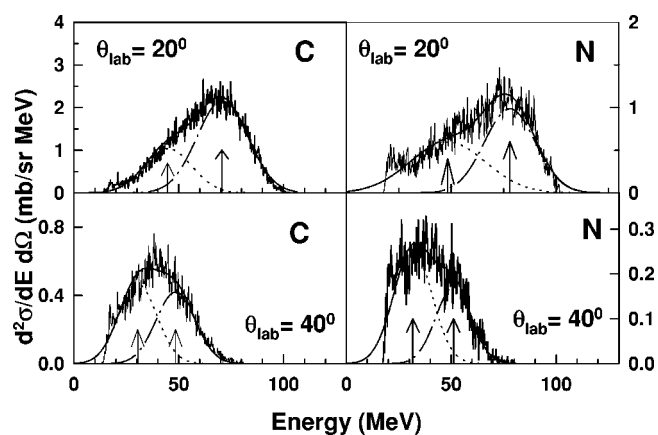

FIG. 2. Energy spectra of carbon and nitrogen fragments at 20° and 40° for the $^{16}O+^{27}Al$ reaction. Dotted, dash-dotted, and solid curves represent contributions of FF, DI, and their sum (FF+DI), respectively. Left and right arrows correspond to the centroids of FF and DI energy distributions, respectively.

The width of the Gaussian was obtained by fitting the lower energy tail of the spectra. The FF component of the energy spectrum thus obtained was then substracted from the full energy spectrum. In the next step, the DI component was obtained by fitting the substracted energy spectra with a second Gaussian. This is illustrated for $^{16}O(116 \text{ MeV})+^{27}Al$ system in Fig. 1, where the extracted FF and DI components for Be, B, C, and N fragments have been displayed (dotted and dash-dotted curves, respectively) along with the experimental data for $\theta_{lab}=15°$. It is clear from Fig. 1 that the experimental energy spectra for all the fragments are nicely fitted with two Gaussians representing FF and DI components. To investigate further the applicability of the scheme over the whole angular range of the data, experimental energy spectra of carbon and nitrogen fragments for the same system at two other angles (20° and 40°) have also been displayed along with the respective estimates of FF and DI components in Fig. 2. It is clear from the figure that in these cases too, the above scheme is fairly successful in estimating the experimental energy spectra. For further illustration, experimental energy spectra of carbon and nitrogen fragments at two different angles for the other systems [i.e., $^{16}O(116 \text{ MeV})+^{28}Si$, $^{20}Ne(145 \text{ MeV})+^{27}Al$, ^{59}Co] have
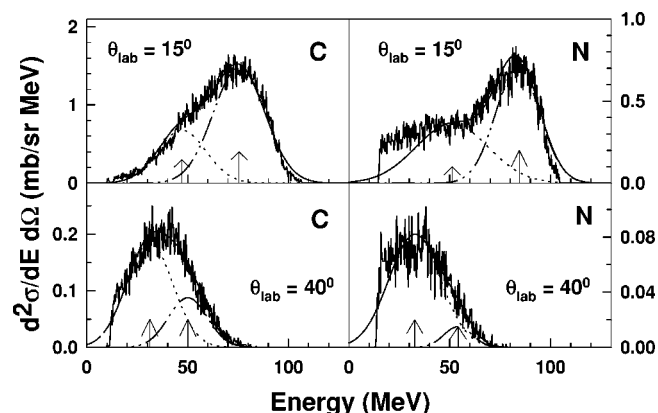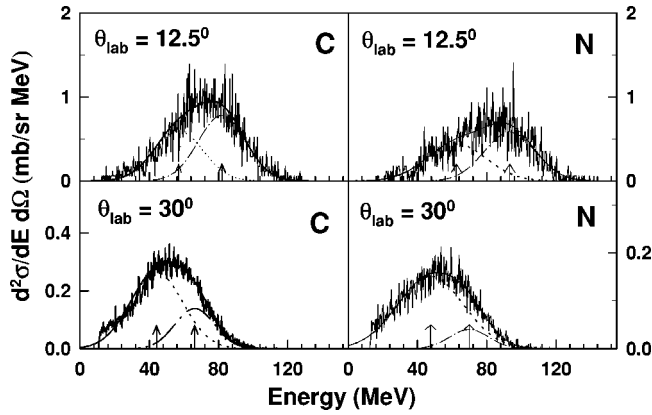

FIG. 3. Same as Fig. 2 at 15° and 40° for the $^{16}O+^{28}Si$ reaction.

FIG. 4. Same as Fig. 2 at 12.5° and 30° for the ^{20}Ne+^{27}Al reaction.

been displayed along with the respective estimates of FF and DI components in Figs. 3, 4, and 5, respectively. It is evident that in all cases the above scheme for the decomposition of FF and DI components works fairly well in estimating the experimental energy spectra.

b. Total elemental yields. The FF and DI components of the total elemental yields, extracted using the procedure outlined above, have been displayed in Fig. 6 for all the reactions under present study. The FF components of the fragment emission cross sections have been compared with the theoretical estimates of the same obtained from the extended Hauser-Feshbach method (EHFM) [22]. The values of the critical angular momentum for fusion l_c and the grazing angular momentum l_g for the systems considered here have been given in Table I. The values of critical angular momenta have been obtained from experimental fusion cross-section data, wherever available [23,24]. Otherwise, they have been obtained from dynamical trajectory model calculations with realistic nucleus-nucleus interaction and dissipative forces generated self-consistently through stochastic nucleon exchanges [25]. The l_c values predicted by the dynamical model have been cross checked with the respective available experimental values and they were found to be in excellent agreement (e.g., for ^{16}O+^{28}Si and ^{20}Ne+^{27}Al systems, predicted values of l_c were 35$\hbar$ and 37$\hbar$, respectively, which

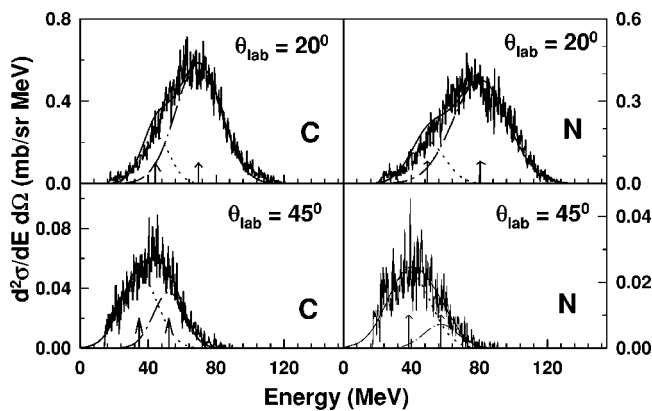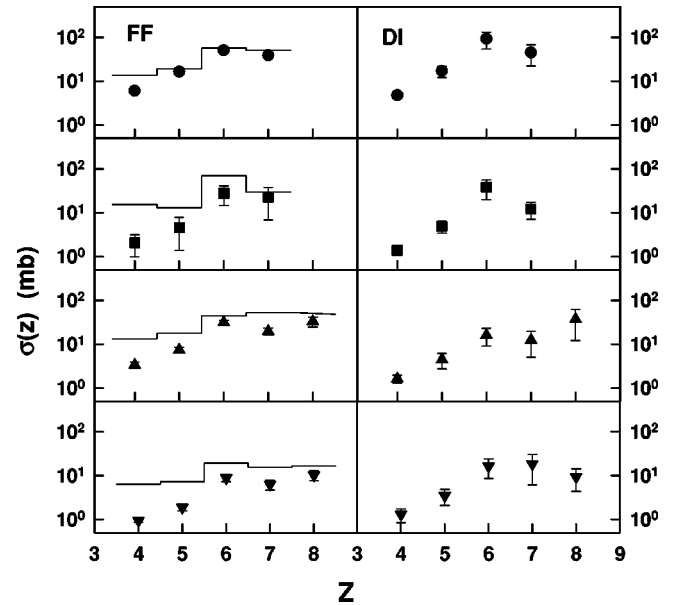FIG. 6. Variation of total elemental yields $\sigma(Z)$ of FF (left) and DI (right) components, plotted as function of fragment charge Z for different systems. Circle, square, triangle, and inverted triangle correspond to the experimental estimates of $\sigma(Z)$ for the reactions ^{16}O(116 MeV)+^{27}Al, ^{16}O(116 MeV)+^{28}Si, ^{20}Ne(145 MeV)+^{27}Al, and ^{20}Ne(145 MeV)+^{59}Co, respectively. The solid histograms are the corresponding EHFM predictions of the total elemental FF yields.

were same as their respective experimental estimates—see Table I). The calculated fragment emission cross sections are shown in Fig. 6 as solid histogram and compared with the experimental estimates of the same (different symbols correspond to different reactions). It is seen from the figure that the theoretical predictions are in fair agreement with the experimental results.

c. Angular distributions. The center of mass angular distributions of FF and DI components for a typical ejectile carbon emitted in the reactions mentioned above have been displayed in Fig. 7 as a function of center of mass angle $\theta_{c.m.}$. The center of mass (c.m.) angular distributions of the FF components, as expected, are found to be symmetric ($\propto 1/\sin \theta_{c.m.}$), whereas those of the DI components are falling off more rapidly indicating shorter lifetime of the dinuclear composite (Fig. 7).

d. Average Q values. The average Q values for the DI

TABLE I. Values of critical and grazing angular momenta (l_c, l_g).

Reaction	l_c	l_g
^{16}O+^{27}Al	34[a]	43
^{16}O+^{28}Si	35[b]	44
^{20}Ne+^{27}Al	37[c]	50
^{20}Ne+^{59}Co	55[a]	63

[a]From theoretical calculation, Ref. [25].
[b]From experimental fusion data, Ref. [23].
[c]From experimental fusion data, Ref. [24].

FIG. 5. Same as Fig. 2 at 20° and 45° for the ^{20}Ne+^{59}Co reaction.
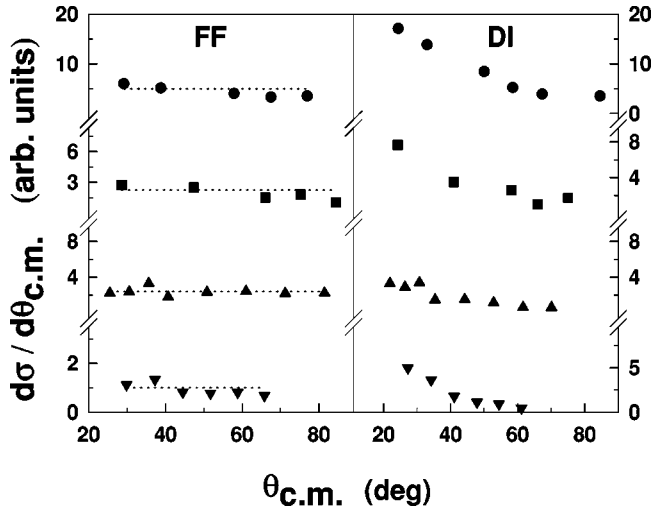
FIG. 7. Variation of cross sections of FF and DI components for carbon fragment, plotted as function of center of mass angle $\theta_{c.m.}$ for different systems. Circle, square, triangle, and inverted triangle correspond to $^{16}O(116 \text{ MeV})+^{27}Al$, $^{16}O(116 \text{ MeV})+^{28}Si$, $^{20}Ne(145 \text{ MeV})+^{27}Al$, and $^{20}Ne(145 \text{ MeV})+^{59}Co$, respectively. The dotted curves correspond to fissionlike angular distribution ($d\sigma/d\Omega \sim a/\sin \theta_{c.m.}$) fit to the FF component of the data.

fragments ($\langle Q_{DI} \rangle$) have been displayed in Fig. 8 as a function of c.m. angle ($\theta_{c.m.}$). The Q values have been estimated from fragment kinetic energies assuming two body kinematics. The fragment kinetic energies were appropriately corrected for particle evaporation from the excited primary fragments assuming thermal equilibrium of the dinuclear composite system. The values of $\langle Q_{DI} \rangle$ for Be and B are found to be nearly constant as a function of angle, whereas those for C and N are found to decrease at forward angles ($\theta_{c.m.} \lesssim 40°$)
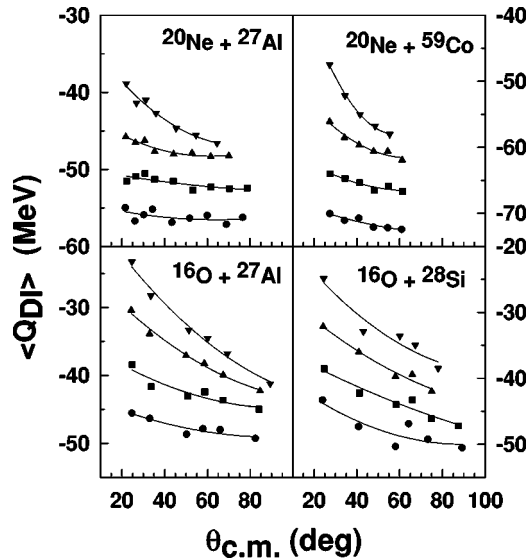

FIG. 8. Variation of optimum Q values for deep inelastic reaction $\langle Q_{DI} \rangle$, plotted as function of center of mass angle $\theta_{c.m.}$ for different systems. Circle, square, triangle, and inverted triangle correspond to the fragments Be, B, C, and N, respectively. Curves are drawn to guide the eye.

and then the two gradually tend to become constant; these imply that, beyond this point, the kinetic energy damping is complete and dynamic equilibrium has been established before the scission of the dinuclear composite takes place. In the following, we try to explore these completely damped collisions further to extract the magnitude of angular momentum damping.

III. DISCUSSION

As mentioned earlier, magnitude of angular momentum damping may be estimated from Eq. (1) only if scission configuration can be estimated independently. Assuming the friction to be at its limit (sticking limit), the extracted scission configuration for $^{20}Ne(120 \text{ MeV})+^{27}Al$ was found to be ~ 11 fm [13], which is much larger than the sum of nuclear radii. However, experimental study of DI collision in the reaction $^{20}Ne(151 \text{ MeV})+^{27}Al$ [10] indicated that scission configuration of the fully damped component (at larger angles) may be quite compact, whereas that for the partially damped component (at smaller angles) may be quite elongated having neck length ~ 3.7 fm. This may be intuitively justified as follows. Deep inelastic collisions are believed to occur within the angular momentum window between the critical angular momentum for fusion l_c and the grazing angular momentum l_g. The partially damped part of it (at forward angles) originate in near peripheral collisions ($l \sim l_g$), which correspond to small overlap and thus a fairly elongated dinuclear configuration; on the other hand, fully damped components (at larger angles) correspond to more compact collisions near $l \sim l_c$. Interestingly, fusion-fission yield is also most predominant in the vicinity of $l \sim l_c$. It is, therefore, likely that the exit channel configurations of both the processes are similar and it appears to be fairly reasonable to assume a compact scission shape for the fully damped component of the data. In the present work, we estimated the scission configuration from the extracted fusion-fission component of the measured fragment energy spectra. The separation distance d between the two fragments at the scission point is calculated from the energy centroid of the FF energy spectra which obeyed Viola systematics [20] corrected for asymmetric mass splitting [21]. The mean values of d thus estimated are; 7.0 ± 0.7 fm for $^{16}O+^{27}Al$, 7.2 ± 0.7 fm for $^{16}O+^{28}Si$, 7.7 ± 1.2 fm for $^{20}Ne+^{27}Al$, and 10.9 ± 1.9 fm for $^{20}Ne+^{59}Co$. Assuming these scission configurations corresponding to each mass splitting to be "frozen," Eq. (1) may then be used to extract the mean angular momentum dissipation factor f in the case of DI collisions. The values of f extracted for different systems are displayed in Fig. 9 (filled circles) along with the rolling and sticking limit predictions (dotted and solid curves, respectively) for the same. For the purpose of evaluation of f, the value of initial angular momentum l_i was taken to be equal to the critical angular momentum for fusion l_c.

It is apparent from Fig. 9 that for all the reactions considered, there is discrepancy between the experimental and empirical estimates of angular momentum dissipation. In all cases, the experimental estimates of the mean angular momentum dissipation are more than their limiting values pre-
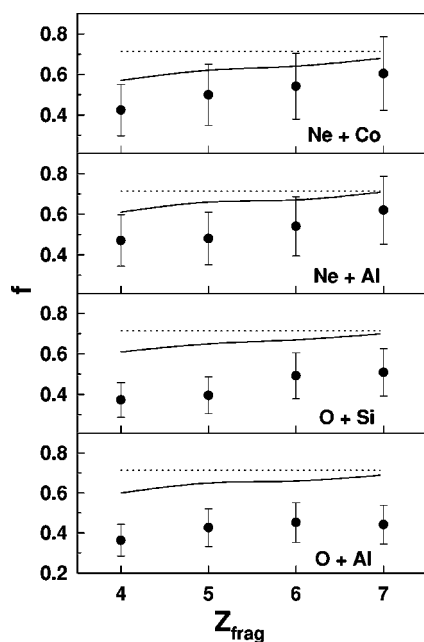
FIG. 9. Variation of angular momentum dissipation factor f with fragment. The filled circles are extracted from the data, solid and dotted curves correspond to sticking limit and rolling limit predictions, respectively.

dicted by the sticking condition (for ^{20}Ne$+^{59}$Co reaction, however, the experimental estimates of f and the corresponding sticking limit predictions are within the ranges of experimental uncertainties). The discrepancy is more for lighter fragments, and gradually decreases for heavier fragments. This may be intuitively understood as follows; it is known from the study of dissipative dynamics of fission (see, for example, Ref. [26] and references therein) that, strong frictional forces in the exit channel cause considerable retardation of the scissioning process leading to increase in scission time scale. As the exit channel configurations of the fully damped DI process are taken to be similar to those for FF process (except that the dinuclear system, in case of DI collision, is formed beyond the conditional saddle point directly), the dynamics of DI process may also experience stronger frictional forces. Microscopically, friction is generated due to stochastic exchange of nucleons between the reacting partners through the window formed by the overlap of the density distributions of the two. Stronger friction, in this scenario, essentially means larger degree of density overlap and more nucleon exchange. Consequently, lighter DI fragments (corresponding to more net nucleon transfer) originate from deeper collisions, for which interaction times are larger. Therefore, angular momentum dissipation too, originating due to stochastic nucleon exchange, may be more which, at least qualitatively, explains the observed trend. Moreover, it is also seen that the difference between the experimental estimates and the corresponding sticking limit predictions is more for lighter systems (^{16}O$+^{27}$Al, ^{28}Si, ^{20}Ne$+^{27}$Al), and

less for the heavier system (^{20}Ne$+^{59}$Co). Qualitatively, this may be due to entrance channel effect [27]; as the formation time (of shape equilibrated fused composite) is smaller for the lighter system at lower spin, the two time scales (of fusion and DI processes) are closer. This may give rise to larger angular momentum dissipation for lighter systems as observed in the present work.

IV. SUMMARY AND CONCLUSIONS

In summary, we have studied fragment emission from ^{16}O(116 MeV)$+^{27}$Al, ^{28}Si, ^{20}Ne(145 MeV)$+^{27}$Al, ^{59}Co reactions and extracted the contributions of fusion-fission and deep inelastic components. Assuming a compact exit channel configuration for the fully damped part of the DI reactions, the exit channel configuration has been estimated from the extracted FF part of the spectra. The angular momentum dissipation for the fully damped DI reactions has then been extracted using these scission shapes. The angular momentum dissipations have been found to be more than the corresponding sticking limit predictions in all the cases except for the case of ^{20}Ne$+^{59}$Co, where the mean values of the experimental estimate of angular momentum dissipation are systematically less than the corresponding sticking limit values, though they are within the range of experimental uncertainty. This may be due to stronger friction in the exit channel which may cause longer overlap of the dinuclear system and consequently more nucleon exchange and dissipation of angular momentum due to stochastic nature of nucleon exchange. The effect is more for lighter systems, as in this case there is more overlap in the time scales of FF and DI processes. However, further systematic studies for each system at different bombarding energies are needed for a better understanding on the dissipation mechanism in light nuclear systems. The inclusive yields for some fragments may have additional contribution from other reaction mechanisms like projectile breakup process (e.g., α breakup in the case of Ne projectile), which should be properly taken care of. The inclusive data presented in this paper may also be useful for future exclusive experiments for which light charged particles are detected in coincidence with either fully damped deep-inelastic or fusion-fission fragments.

[1] C. Bhattacharya, K. Mullick, S. Bhattacharya, K. Krishan, T. Bhattacharjee, P. Das, S. R. Banerjee, D. N. Basu, A. Ray, S. K. Basu, and M. B. Chatterjee, Phys. Rev. C **66**, 047601 (2002).

[2] A. A. P. Suaide *et al.*, Phys. Rev. C **66**, 014607 (2002).

[3] S. J. Sanders, A. Szanto de Toledo, and C. Beck, Phys. Rep. **311**, 487 (1999).

[4] I. Berceanu *et al.*, Phys. Rev. C **57**, 2359 (1998).

[5] C. Beck *et al.*, Eur. Phys. J. A **2**, 281 (1998).

[6] C. Beck *et al.*, Phys. Rev. C **54**, 227 (1996).

[7] C. Beck, B. Djerroud, F. Haas, R. M. Freeman, A. Hachem, B. Heusch, A. Morsad, M. Vuillet-A-Cilles, and S. J. Sanders, Phys. Rev. C **47**, 2093 (1993).

[8] C. Beck *et al.*, Z. Phys. A: Hadrons Nucl. **343**, 309 (1992).

[9] E. A. Bakkum, P. Decowski, K. A. Griffioen, R. J. Meijer, and R. Kamermans, Nucl. Phys. **A511**, 117 (1990).

[10] Nguyen Van Sen, R. Darves-Blanc, J. C. Gondrand, and F. Merchez, Phys. Rev. C **27**, 194 (1983).

[11] D. Shapira, R. Novotny, Y. D. Chan, K. A. Erb, J. L. C. Ford, J. C. Peng, and J. D. Moses, Phys. Lett. **114B**, 111 (1982).

[12] D. Shapira, J. L. C. Ford, and J. Gomez del Campo, Phys. Rev. C **26**, 2470 (1982).

[13] J. B. Natowitz, M. N. Namboodiri, R. Eggers, P. Gonthier, K. Geoffroy, R. Hanus, C. Towsley, and K. Das, Nucl. Phys. **A277**, 477 (1977).

[14] R. Eggers, M. N. Namboodiri, P. Gonthier, K. Geoffroy, and J. B. Natowitz, Phys. Rev. Lett. **37**, 324 (1976).

[15] T. M. Cormier *et al.*, Phys. Rev. C **13**, 682 (1976).

[16] T. M. Cormier, P. Braun-Munzinger, P. M. Cormier, J. W. Harris, and L. L. Lee, Phys. Rev. C **16**, 215 (1977).

[17] R. R. Betts and S. B. DiCenzo, Phys. Rev. C **19**, 2070 (1979).

[18] P. Braun-Munzinger, T. M. Cormier, and C. K. Gelbke, Phys. Rev. Lett. **37**, 1582 (1976).

[19] A. Szanto de Toledo *et al.*, Phys. Rev. C **56**, 558 (1997).

[20] V. E. Viola, K. Kwiatkowski, and M. Walker, Phys. Rev. C **31**, 1550 (1985).

[21] C. Beck and A. Szanto de Toledo, Phys. Rev. C **53**, 1989 (1996).

[22] T. Matsuse, C. Beck, R. Nouicer, and D. Mahboub, Phys. Rev. C **55**, 1380 (1997).

[23] P. Papka *et al.*, Acta Phys. Pol. B **34**, 2343 (2003).

[24] B. Djerroud, Ph.D. thesis, University Louis Pasteur, Strasbourg, 1992 (unpublished).

[25] S. Bhattacharya, K. Krishan, S. K. Samaddar, and J. N. De, Phys. Rev. C **37**, 2916 (1988).

[26] A. K. Dhara, K. Krishan, C. Bhattacharya, and S. Bhattacharya, Phys. Rev. C **57**, 2453 (1998).

[27] A. Szanto de Toledo, B. V. Carlson, C. Beck, and M. Thoennessen, Phys. Rev. C **54**, 3290 (1996).